Possible mechanisms of polyphosphate-induced amyloid fibril formation of β_2-microglobulin

Chun-ming Zhang[a,1], Keiichi Yamaguchi[a,1], Masatomo So[a], Kenji Sasahara[a], Toru Ito[b], Suguru Yamamoto[b], Ichiei Narita[b], József Kardos[c], Hironobu Naiki[d], and Yuji Goto[a,2]

[a]Institute for Protein Research, Osaka University, Suita, 565-0871 Osaka, Japan; [b]Division of Clinical Nephrology and Rheumatology, Niigata University Graduate School of Medical and Dental Sciences, 951-8510 Niigata, Japan; [c]ELTE NAP Neuroimmunology Research Group, Department of Biochemistry, Eötvös Loránd University, 1117 Budapest, Hungary; and [d]Faculty of Medical Sciences, University of Fukui, Matsuoka, 910-1193 Fukui, Japan

Edited by Susan Marqusee, University of California, Berkeley, CA, and approved May 14, 2019 (received for review November 20, 2018)

Polyphosphate (polyP), which is found in various microorganisms and human cells, is an anionic biopolymer consisting of inorganic phosphates linked by high-energy phosphate bonds. Previous studies revealed that polyPs strongly promoted the amyloid formation of several amyloidogenic proteins; however, the mechanism of polyP-induced amyloid formation remains unclear. In the present study using β_2-microglobulin (β2m), a protein responsible for dialysis-related amyloidosis, we investigated amyloid formation in the presence of various chain lengths of polyPs at different concentrations under both acidic (pH 2.0 to 2.5) and neutral pH (pH 7.0 to 7.5) conditions. We found that the amyloid formation of β2m at acidic pH was significantly accelerated by the addition of polyPs at an optimal polyP concentration, which decreased with an increase in chain length. The results obtained indicated that electrostatic interactions between positively charged β2m and negatively charged polyPs play a major role in amyloid formation. Under neutral pH conditions, long polyP with 60 to 70 phosphates induced the amyloid formation of β2m at several micromoles per liter, a similar concentration range to that in vivo. Since β2m with an isoelectric point of 6.4 has a slightly negative net charge at pH 7, polyPs were unlikely to interact with β2m electrostatically. PolyPs appear to dehydrate water molecules around β2m under the unfolded conformation, leading to the preferential stabilization of less water-exposed amyloid fibrils. These results not only revealed the pH-dependent mechanism of the amyloid formation of β2m but also suggested that polyPs play an important role in the development of dialysis-related amyloidosis.

amyloid fibrillation | amorphous aggregation | dialysis-related amyloidosis | polyphosphates | supersaturation

Aggregates of denatured proteins may be classified into two types: amyloid fibrils and amorphous aggregates (1–5). Amyloid fibrils, in which β-strands are aligned perpendicularly to the fibril's axis (6, 7), are associated with a wide range of human diseases, such as Alzheimer's disease, Parkinson's disease, and dialysis-related amyloidosis (8, 9). Amorphous aggregates without an ordered β-sheet structure are common to denatured proteins and are also associated with diseases such cataracts caused by α-crystallin aggregation (10). We proposed that amyloid fibrils and amorphous aggregates are similar to the crystals and amorphous aggregates (or glass) of solutes or substances (1, 2, 5, 11). We suggested a competitive mechanism of protein aggregation in which supersaturation-limited amyloid formation competes with supersaturation-unlimited amorphous aggregation, to obtain a more comprehensive understanding of protein aggregation (1, 2, 5, 11).

To address the mechanism of protein aggregation accommodating both amyloidogenic and nonamyloidogenic aggregates, the effects of additives, including various salts, have been investigated (12–14). Polyphosphate (polyP) (Fig. 1*A*), a biopolymer consisting of phosphate groups linked by high-energy phosphoanhydride bonds, was more recently reported to induce the amyloid fibrils of several amyloidogenic proteins (15). PolyPs are frequently found in nature, including microorganisms and mammals (16, 17), and are assumed to be essential for organisms to live and mainly function as a reservoir of phosphate groups. In rodent tissues (the brain, heart, kidneys, liver, and lungs), polyP concentrations are 25 to 120 μM in phosphate units with an average length of ∼50 to 800 phosphate units (16). PolyPs with 70 to 75 phosphates have been identified at a concentration of 1.1 mM in phosphate units in the human platelets (18). PolyPs released from activated platelets accelerate blood clotting by the thrombin stimulation (18, 19). After full platelet activation, human blood contains 1 to 3 μM polyP (20). However, the mechanism underlying polyP-induced amyloid formation remains unclear.

β_2-Microglobulin (β2m), which consists of 99 amino acid residues, is a light chain of major histocompatibility complex class I (8, 21). β2m is steadily metabolized and degraded in the kidneys after being released into the blood. In hemodialysis patients, the concentration of β2m increases up to 50 mg/L because it is not degraded in patients with kidney disorders and cannot pass through a dialysis membrane (8, 21). Amyloid fibrils of β2m are deposited in the peritenons and synovial membranes of the carpal tunnel, causing dialysis-related amyloidosis, a serious complication of long-term hemodialysis therapy (8, 21). Nevertheless, the risk for dialysis-related amyloidosis in Japan decreased significantly from 1998 to 2010, suggesting that improvements in dialysis technology, in particular, introduction of membranes that reduce β2m in blood, contributed significantly to the decreased risk (22).

In vitro studies on the amyloid formation of β2m have been extensively performed under acidic pH conditions, under which β2m was unfolded and easily converted into amyloid fibrils (1, 23–25). In contrast, amyloid formation under neutral pH conditions, under which patients develop diseases, did not occur easily

Significance

Although amyloid fibrils are associated with numerous pathologies, the factors triggering amyloid formation remain largely unknown. Polyphosphates were recently reported to induce amyloid fibrils of several amyloidogenic proteins. We found that, under both acidic and neutral pH conditions, the amyloid formation of β_2-microglobulin was significantly accelerated by polyphosphates. We elucidated the underlying pH-dependent mechanisms, which will be important for a more comprehensive understanding of the amyloid formation of proteins. Due to the marked ability of polyphosphates to induce the amyloid formation of β_2-microglobulin, even at neutral pH, polyphosphates may play an important role in the development of dialysis-related amyloidosis.

Author contributions: K.Y., M.S., T.I., S.Y., I.N., J.K., H.N., and Y.G. designed research; C.-m.Z., K.Y., M.S., and K.S. performed research; C.-m.Z., K.Y., M.S., and K.S. analyzed data; and C.-m.Z., K.Y., M.S., K.S., T.I., S.Y., I.N., J.K., H.N., and Y.G. wrote the paper.

The authors declare no conflict of interest.

This article is a PNAS Direct Submission.

[1]C.-m.Z. and K.Y. contributed equally to this work.

[2]To whom correspondence may be addressed. Email: gtyj8126@protein.osaka-u.ac.jp.

This article contains supporting information online at www.pnas.org/lookup/suppl/doi:10.1073/pnas.1819813116/-/DCSupplemental.

Published online June 10, 2019.

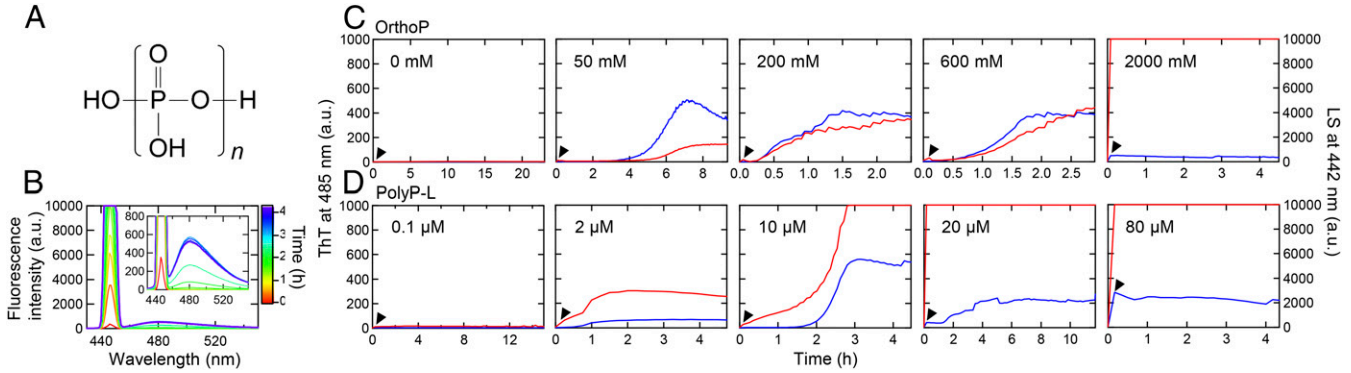

Fig. 1. PolyP-induced amyloid formation of β2m at acidic pH. (*A*) Chemical structure of polyP. *n* is the degree of polymerization of the phosphate group. (*B*) Repeated measurements of spectra with an excitation at 445 nm in the presence of polyP-L. *Inset* shows an expanded image of ThT fluorescence. (*C* and *D*) Kinetics of amyloid formation monitored by ThT fluorescence at 485 nm (blue) and total aggregation monitored by LS at 442 nm (red) at various concentrations of orthoP (*C*) and polyP-L (*D*) at 37 °C under ultrasonication. β2m was added at the time indicated by the arrowhead.

because of the stable native conformation (13, 26). Based on previous studies performed with N-terminal truncated or mutant β2m (13, 27) or those in the presence of additives, such as collagen, heparin (28), sodium dodecyl sulfate (SDS) (29), or glycosaminoglycans (21), the denaturation or local enrichment of β2m on biological membranes or extracellular matrix molecules has been suggested to trigger amyloid formation in vivo. However, the mechanism of amyloid formation in patients under neutral pH conditions remains unclear.

We herein investigated the amyloid formation of β2m in the presence of various chain lengths of polyPs. Orthophosphate (orthoP), diphosphate (diP), tetraphosphate (tetraP), short polyphosphates with 10 to 15 phosphate groups (polyP-S), and long polyphosphates with 60 to 70 phosphate groups (polyP-L) were used to systematically examine the amyloid formation of β2m under acidic and neutral pH conditions. To accelerate supersaturation-limited amyloid formation, we performed experiments under ultrasonic irradiation (1, 2, 5). We found that, under both acidic and neutral pH conditions, the amyloid formation of β2m was significantly accelerated by polyPs. The results obtained revealed the underlying pH-dependent distinct mechanisms: under acidic pH conditions, attractive charge–charge interactions between positively charged β2m and negatively charged polyPs accelerated amyloid formation, whereas the preferential stabilization of amyloid fibrils in the presence of dehydrating polyP anions played a major role under neutral pH conditions.

Results

PolyP-Induced Amyloid Formation of β2m at Acidic pH. Amyloid formation of β2m in the presence of various concentrations (0 to 2.0 M) of orthoP in 10 mM HCl (pH 2.0 to 2.5) was monitored by thioflavin T (ThT) fluorescence and light scattering (LS), at 485 and 442 nm, respectively, upon exiting at 445 nm (Fig. 1*B* and *SI Appendix*, *Supplementary Materials and Methods*). Because ThT fluorescence specifically detects amyloid fibrils, while LS detects the total amount of aggregates, including amyloid fibrils and amorphous aggregates, we can distinguish amyloid formation and amorphous aggregation. In the presence of 50 mM orthoP, ThT fluorescence and LS intensities both increased after a lag time of 4.5 h, although no significant change occurred in the absence of orthoP during an incubation period of 24 h (Fig. 1*C*). At 200 or 600 mM orthoP, ThT fluorescence and LS intensities increased with a lag time of ∼0.5 h. In contrast, at 2.0 M orthoP, only LS intensity immediately increased with the addition of β2m monomers into the reaction mixture, which indicated amorphous aggregation without amyloid fibrils.

We then examined the effects of polyP-L with 60 to 70 phosphates. ThT and LS intensities both increased markedly at a polyP-L concentration as low as 2 μM (Fig. 1*D*). At 10 μM polyP-L, LS markedly increased, and this was followed by an increase in ThT fluorescence after a lag time of 2 h. In the presence of 20 or 80 μM polyP-L, LS intensity increased above the detection limit immediately after starting the reaction, indicating that rapid amorphous aggregation dominated.

We also investigated the effects of polyPs with various chain lengths between orthoP and polyP-L, i.e., diP, tetraP, and polyP-S with 10 to 15 phosphates (*SI Appendix*, Fig. S1). Although low concentrations of polyPs effectively induced amyloid fibrils, high concentrations induced amorphous aggregates. At certain concentration ranges (Fig. 2 and *SI Appendix*, Fig. S1 *B* and *C*), we observed a rapid increase in LS followed by a delayed increase in ThT fluorescence after a lag time, indicating kinetic competition between rapid amorphous aggregation or oligomer formation and the slow conversion to amyloid fibrils, as predicted by the competitive mechanism of amorphous aggregation and amyloid formation (1, 2, 5, 11). However, we have no structural or morphological evidence for transient amorphous aggregation, and further studies are required to verify this.

The effectiveness of polyPs at accelerating amyloid formation critically depend on chain lengths:

$$\text{polyP-L} > \text{polyP-S} > \text{tetraP} > \text{diP} > \text{orthoP}. \quad [1]$$

We plotted the maximum values of ThT fluorescence and LS intensities after the conformational transition against polyP concentrations (Fig. 2*A*). ThT fluorescence reached a maximum at 100 mM orthoP and gradually decreased at a concentration higher than 200 mM orthoP. LS intensity gradually increased and exceeded the detection limit at 2 M orthoP, at which amorphous aggregates dominated. Previous studies showed that although low concentrations of NaCl produced amyloid fibrils, high concentrations of NaCl (e.g., 1.0 M) produced amorphous aggregates, making an optimum for amyloid formation at ∼0.2 M NaCl (1, 2, 5, 12). Thus, the effects of orthoP on amyloid formation are similar to those of NaCl, although amyloid fibrils remained even at 1 M orthoP. ThT fluorescence in the presence of diP, tetraP, polyP-S, and polyP-L reached a maximum at ∼10 mM, 0.2 mM, 100 μM, and 10 μM, respectively, and then gradually decreased (Fig. 2*A*). In contrast, LS continued to increase and often exceeded the detection limit, suggesting that amorphous aggregates prevailed.

Transmission electron microscopy (TEM) showed that the amyloid fibrils that formed in the presence of polyPs in 10 mM HCl were straight with a diameter of 10 to 15 nm and were slightly fragmented by ultrasonic irradiation (Fig. 2 *B*, *Inset*). We observed small amorphous aggregates coexisted particularly at 10 mM diP and 100 μM polyP-S. Amorphous aggregates were observed at high polyP concentrations: 2 M orthoP, 1 M diP, 2 mM tetraP, 1 mM polyP-S, or 80 μM polyP-L (*SI Appendix*, Fig. S2).

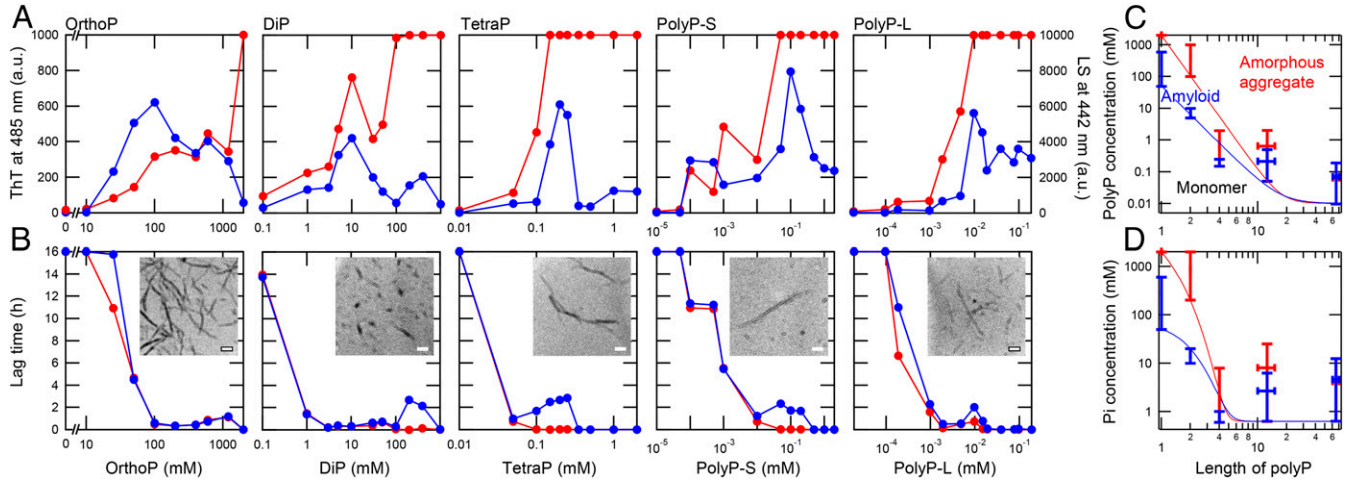

Fig. 2. Amyloid formation in the presence of various types of polyPs. (*A*) Maximum values of ThT fluorescence (blue) and LS (red) at acidic pH (10 mM HCl) in the presence of orthoP, diP, tetraP, polyP-S, and polyP-L. (*B*) Lag times of ThT fluorescence (blue) and LS (red) in the presence of orthoP, diP, tetraP, polyP-S, and polyP-L. *Insets* show TEM images of amyloid fibrils formed at 100 mM orthoP, 10 mM diP, 0.2 mM TetraP, 100 μM polyP-S, and 10 μM polyP-L. (Scale bars, 200 nm.) (*C* and *D*) Phase diagrams for the polyP-induced aggregation of β2m. The aggregation of β2m depending on concentrations of polyP units (*C*) and inorganic phosphate (Pi) units (*D*) as a function of the chain length of polyP. PolyP concentrations showing ThT fluorescence of more than 300 (blue bars) and LS exceeding the detection limit (red bars) at acidic pH in A are plotted. The boundary lines between monomer and amyloid and between amyloid and amorphous aggregate are depicted in blue and red, respectively.

We also examined the secondary structure of β2m aggregates using circular dichroism (CD) spectroscopy (*SI Appendix*, *Supplementary Results* and Fig. S3). Although CD spectra showed that soluble β2m at low concentrations of polyPs assumed a disordered conformation, they were converted to a β-sheet–rich amyloid conformation with a minimum at ∼213 to 220 nm, which is consistent with the transition monitored by ThT. At higher concentrations of polyPs, CD intensities decreased to almost zero, indicating the formation of amorphous aggregates (*SI Appendix*, Fig. S3).

Lag times monitored by ThT fluorescence and LS in the presence of low concentrations of orthoP, diP, tetraP, polyP-S, and polyP-L agreed well (Fig. 2*B*). However, a clearer delay in the lag time monitored by ThT fluorescence than that monitored by LS was observed at high concentrations of polyPs. These results indicated that polyP-dependent rapid amorphous aggregation kinetically competed with the slow formation of amyloid fibrils, producing a kinetic complexity predicted by the competitive mechanism of amyloid formation (1, 2, 5).

PolyP-Induced Amyloid Formation at Neutral pH. We investigated the amyloid formation of β2m at neutral pH (pH 7 to 7.5) using tetraP, polyP-S, and polyP-L at concentrations of 200, 100, and 20 μM, respectively, which were the optimal concentrations for fibril formation at acidic pH. ThT fluorescence significantly increased in the presence of 20 μM polyP-L after an incubation for 25 h (*SI Appendix*, Fig. S4 *A* and *B*). The intensity of ThT fluorescence at neutral pH was approximately 10-fold stronger than that at acidic pH, exceeding the detection limit after an incubation for 30 h. It is possible that the intrinsic increase in ThT fluorescence at neutral pH contributes to the observed strong ThT fluorescence. At fivefold higher concentrations of tetraP, polyP-S, and polyP-L, ThT fluorescence slightly increased for tetraP (1 mM) and polyP-S (0.5 mM) and significantly increased for polyP-L (0.1 mM) (*SI Appendix*, Fig. S4 *C* and *D*). TEM observations showed that β2m formed a large number of straight fibrils at 0.1 mM polyP-L (Fig. 3*A*), while a small number of fibrils were observed at 1 mM tetraP and 0.5 mM polyP-S (*SI Appendix*, Fig. S4*E*). The amyloid fibrils that formed at neutral pH with a diameter of 10 to 25 nm, particularly those in the presence of polyP-S (*SI Appendix*, Fig. S4*E*) or polyP-L (Fig. 3*A*), were thicker than those that formed at acidic pH with a diameter of 10 to 15 nm (Fig. 2 *B*, *Insets*).

We focused on amyloid formation in the presence of polyP-L at various concentrations at neutral pH (Fig. 3). Even at 2 μM polyP-L, ThT fluorescence increased after a lag time of 15 h (Fig. 3*A*). At 100 μM polyP-L, ThT exceeded the detection limit of 10,000 (arbitrary units). At a high concentration of polyP-L (2 mM), ThT fluorescence was lower than those at lower polyP-L concentrations. Regarding all concentrations of polyP-L, LS and ThT fluorescence increased simultaneously, which was distinct from the separate increases observed at acidic pH (Fig. 1 and *SI Appendix*, Fig.S1). The plots of the maximum values of ThT fluorescence and LS intensities against polyP-L concentrations showed that ThT fluorescence and LS increased at a concentration of 1 μM and then both decreased at ∼1 mM (Fig. 3*B*). The lag times showed that amyloid formation was promoted at 1 to 1,000 μM polyP-L (Fig. 3*C*).

The CD spectrum showed that β2m formed a native β-sheet conformation in the absence of polyP-L at neutral pH (Fig. 3 *D* and *E*). In the presence of polyP-L at 10 μM to 2 mM, β2m exhibited CD spectra with a large minimum at ∼220 nm, indicating that β2m formed typical β-rich amyloid fibrils. The CD spectrum at 8 mM polyP-L showed the native-like β-sheet conformation, which is consistent with the assumption that competition between the stabilization of the native state and induction of amyloid fibrils occurred at high polyP-L concentrations.

As a comparison, we measured the amyloid formation of β2m in the presence of 0.5 mM SDS at pH 7.0 with ultrasonication, where β2m readily formed amyloid fibrils since SDS partially destabilized the native conformation of β2m (Fig. 3*F*) (29). The lag time of 2.5 h was markedly shorter than that of polyP-L–dependent amyloid formation. TEM revealed highly associated amyloid fibrils (Fig. 3*F*, *Inset*). Even without ultrasonication, polyP-L at 20 or 1,000 μM induced amyloid formation (Fig. 3*G*). Although they showed weak ThT fluorescence and LS intensities, TEM confirmed the straight and rigid amyloid fibrils (Fig. 3*G*, *Inset*).

Interaction between polyPs and β2m Revealed by Isothermal Titration Calorimetry Experiments. To examine the affinity between polyPs and β2m, we performed isothermal titration calorimetry (ITC) experiments under acidic and neutral pH conditions using tetraP and polyP-L. At acidic pH, the titration of tetraP or polyP-L with β2m showed a saturating titration curve, with the strength of the interaction for polyP-L being stronger than that for tetraP (Fig. 4*A*). However, the exothermic heat effect observed for each injection of

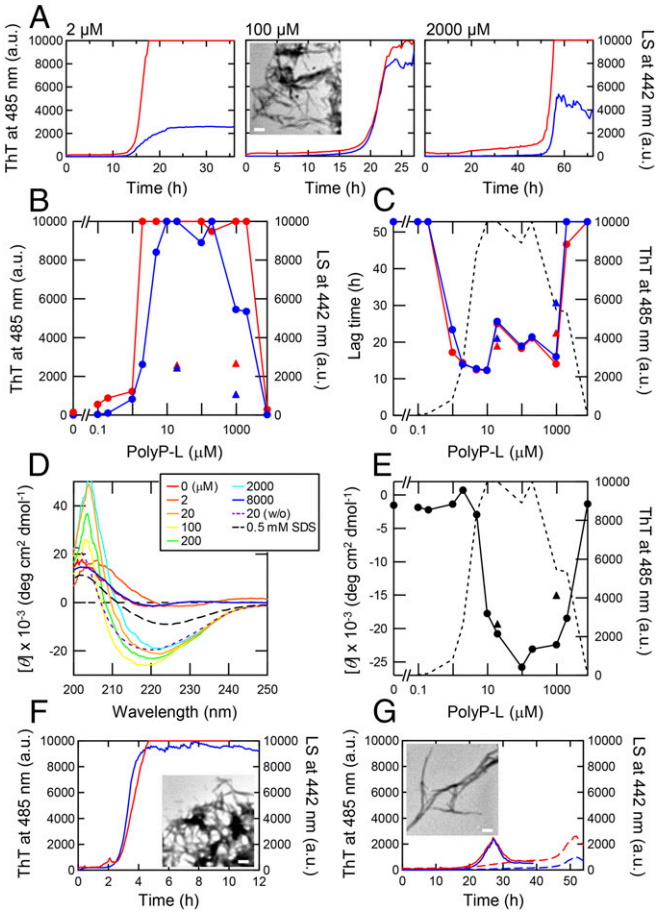

Fig. 3. PolyP-L–induced amyloid formation of β2m at neutral pH. (*A*) Kinetics of amyloid formation monitored by ThT fluorescence at 485 nm (blue) and aggregation monitored by LS at 442 nm (red) at concentrations of 2, 100, and 2,000 μM polyP-L at 37 °C. A TEM image of amyloid fibrils formed at 100 μM polyP-L is shown. (Scale bars, 200 nm.) (*B* and *C*) Maximum values of ThT fluorescence at 485 nm (blue circles), LS at 442 nm (red circles) (*B*), and lag time (*C*) at various concentrations of polyP-L. In *C* and *E*, the dotted line represents the maximum ThT fluorescence in *B*. (*D*) CD spectra obtained after amyloid formation at various concentrations of polyP-L. Dotted line shows CD spectrum in polyP-L without ultrasonication. The dashed line shows CD spectrum in 0.5 mM SDS with ultrasonication. (*E*) CD ellipticities at 220 nm with ultrasonication (solid circles) and without ultrasonication (solid triangles) at various concentrations of polyP-L. (*F* and *G*) Kinetics of amyloid formation monitored by ThT fluorescence (blue) and aggregation monitored by LS (red) at 0.5 mM SDS with ultrasonication (*F*) and at 20 (solid lines) and 1,000 μM (dashed lines) polyP-L without ultrasonication (*G*). *Insets* show EM images of amyloid fibrils formed at 0.5 mM SDS with ultrasonication (*F*) and 20 μM polyP-L without ultrasonication (*G*). (Scale bars, 200 nm.)

β2m was independent of polyP concentrations, suggesting that affinity was independent of polyP concentrations. The stoichiometry of binding was 1 mol of β2m interacting with 19.8 mol of tetraP and 2.2 mol of polyP-L with a dissociation constant, K_D, of 13.0 and 7.5 nM, respectively, revealing exothermic strong binding (Fig. 4 *C* and *D*). The enthalpy change (ΔH) and free energy change (ΔG) for binding were −121.5 and −45.0 kJ/mol for tetraP, respectively, and −137.2 and −46.0 kJ/mol for polyP-L, respectively (Fig. 4*G*). TetraP and polyP-L contained 4 and 60 to 70 negative charges, respectively, and β2m had a net charge of +18 at pH 2. The larger number of binding sites for tetraP (19.8 mol) than polyP-L (2.2 mol) was consistent with the dominant role of electrostatic interactions.

In contrast, at neutral pH, under which polyPs and β2m were both negatively charged, the titration of tetraP or polyP-L with β2m showed endothermic heat (Fig. 4 *B*, *E*, *F*, and *H*). Endothermic heat was not observed when β2m was titrated into a solution without polyPs (*SI Appendix*, Fig. S5). The apparent stoichiometry of binding tentatively obtained assuming a binding mechanism was 1 mol of β2m interacting with 41.7 mol of tetraP with K_D of 3.7 μM, respectively (Fig. 4*E*). The ΔH and ΔG values for binding were 220.1 and −31.0 kJ/mol, respectively (Fig. 4*H*). Thermodynamic parameters indicated that the driving force for favorable ΔG arises from the positive entropy change (ΔS), implying that the dehydration of water molecules around β2m occurred upon the mixing of polyPs and β2m.

We measured ^{1}H-^{15}N heteronuclear single quantum coherence NMR spectra of β2m in the presence and absence of 20 μM polyP-L (*SI Appendix*, Fig. S6). However, no chemical shift perturbation was observed for any cross-peaks. Thus, direct binding between β2m and polyP-L at neutral pH was not observed by NMR as well as ITC experiments.

Effects of PolyPs on the Conformational States. We examined the stability of native β2m monomers at neutral pH in the presence of various concentrations of polyP-L by performing thermal or urea-induced unfolding experiments (*SI Appendix*, *Supplementary Results*, Fig. S7 *A* and *C*, and Table S1). However, the stabilizing effect of polyP-L on β2m was not observed for either. As a model compound with strong Hofmeister salting-out effects, we also investigated the effects of $(NH_4)_2SO_4$ on the urea-induced unfolding of β2m (*SI Appendix*, Fig. S7*B* and Table S1). As reported previously with $(NH_4)_2SO_4$ (30), the addition of $(NH_4)_2SO_4$ stabilized β2m against urea-induced unfolding.

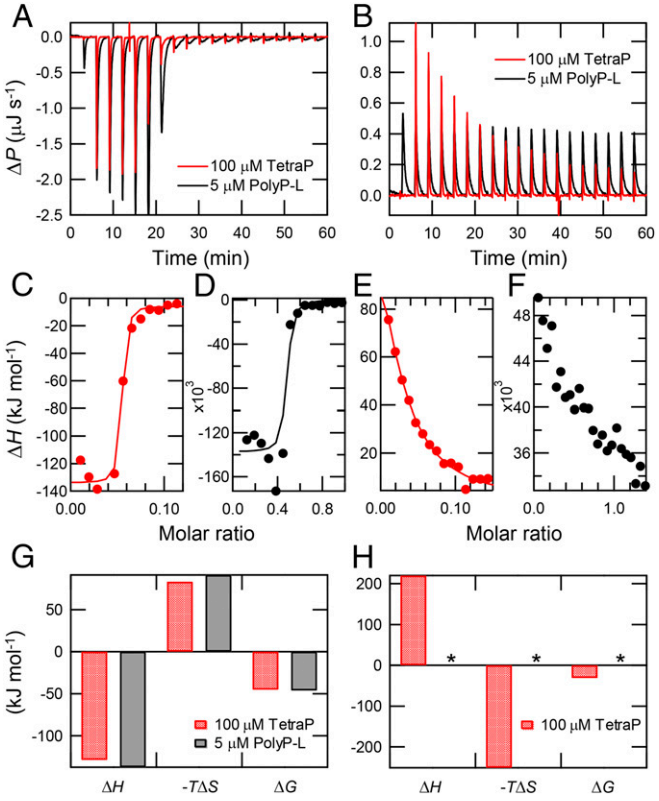

Fig. 4. Interaction between polyPs and β2m revealed by ITC experiments. (*A* and *B*) Direct heat effects for the injection of β2m into 100 μM tetraP (red) and 5 μM polyP-L (black) under acidic (*A*) and neutral (*B*) pH conditions. (*C*–*F*) Total heat effects (ΔH) for each injection at 100 μM tetraP (*C* and *E*) and 5 μM polyP-L (*D* and *F*) under acidic (*C* and *D*) and neutral (*E* and *F*) pH conditions. (*G* and *H*) Thermodynamic parameters (ΔH, $-T\Delta S$, and ΔG) at acidic (*G*) and neutral (*H*) conditions, respectively. Parameters not assessed because of a poor fit are indicated by asterisks.

Amyloid fibrils of β2m that form at acidic pH are known to depolymerize with increases in pH to neutral pH (23, 26). We examined the effects of polyP-L on the depolymerization of preformed fibrils at acidic pH (*SI Appendix*, Fig. S7*D*). We observed the marked retardation of depolymerization in the presence of polyP-L, suggesting that polyPs stabilize amyloid fibrils, thereby changing the conformational equilibria toward amyloid fibrils. Similar stabilizing effects have been reported for other biological additives, including glycosaminoglycans, proteoglycans, and lipids (21).

Discussion

Possible Effects of PolyPs on Amyloid Formation. Considering the presence of a large number of negatively charged phosphate groups, the marked effects of polyPs on the amyloid formation of β2m may be caused by the salt effects. Three major mechanisms generally participate in salt or ion effects on proteins (31, 32).

The first is the Debye–Hückel ion screening effect, which is proportional to the square root of ionic strength, independent of salt species, and generally plays a role at low ion concentrations.

The second is the Hofmeister effect, in which water structure-making kosmotropic ions (e.g., fluoride or sulfate anions) exert stronger effects than water structure-breaking chaotropic ions on protein stabilization, precipitation, and crystallization. For an example, a Hofmeister series for anions (33) is:

$$\begin{aligned}\text{Sulfate}^{2-} > \text{phosphate}^{2-} > \text{fluoride}^{-} > \text{chloride}^{-} > \text{bromide}^{-} \\ > \text{iodide}^{-} > \text{perchlorate}^{-} > \text{thiocyanate}^{3-}.\end{aligned} \quad [2]$$

The third is the counter ion-binding effect, which follows the electroselectivity series representing the affinities of charge–charge interactions. An electroselectivity series for anions to positively charged groups is:

$$\begin{aligned}\text{Sulfate}^{2-} > \text{perchlorate}^{-} > \text{thiocyanate}^{-} > \text{iodide}^{-} > \text{nitrate}^{-} \\ > \text{bromide}^{-} > \text{chloride}^{-} > \text{acetate}^{-} = \text{fluoride}^{-}.\end{aligned} \quad [3]$$

These three types of salt or ion effects on proteins may be distinguished from the concentration range and order of effectiveness of various salts or ions (31, 32).

Mechanism of PolyP-Induced Amyloid Formation under Acidic Conditions. Charge–charge interactions clearly contribute to the effects of polyPs under acidic conditions, under which acid-denatured proteins are highly positively charged and polyPs are highly negatively charged (Fig. 5). To demonstrate the role of the charge–charge interaction, we made a phase diagram of acid-denatured β2m monomers, amyloid fibrils, and amorphous aggregates dependent on polyP concentrations (mM) and polyP lengths (Fig. 2 *C* and *D*).

Regarding orthoP and diP, the maximum value of ThT fluorescence was observed at a phosphate concentration that was approximately 10-fold lower than that for the detection limit of LS, separating the phases for amyloid fibrils and amorphous aggregates, with the former clearly being observed at the lower concentrations of orthoP and diP. The clear separation of the amyloid and amorphous phases was not observed for tetraP, polyP-S, or polyP-L. However, kinetics for DiP, TetraP, PolyP-S, and PolyP-L monitored by ThT were slower than those monitored by LS, indicating competition between rapid amorphous aggregation and supersaturation-limited slow amyloid formation (Fig. 2*B*). Thus, polyP-dependent amyloid formation under acidic conditions follows a competitive mechanism between amyloid fibrils and amorphous aggregates, as established for β2m with various salts (1, 2, 5) and additives, including SDS (24) and heparin (25).

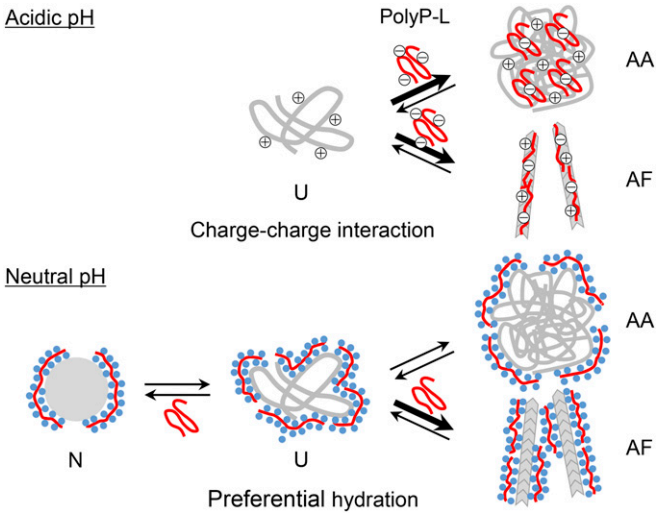

Fig. 5. Schematic models of the interaction between polyPs and β2m. At acidic pH, the electrostatic interaction between polyPs and unfolded β2m (U) stabilized amyloid fibrils (AF) and amorphous aggregates (AA) competitively depending on the concentration of polyPs. At neutral pH, under which β2m and polyPs were both negatively charged, hydration around the phosphate groups of polyP led to the preferential stabilization of dehydrated amyloid fibrils over amorphous aggregates. Although the native state was also likely to be stabilized, the net effects shifted the equilibrium toward the formation of amyloid fibrils.

Mechanism of PolyP-Induced Amyloid Formation under Neutral pH Conditions. Attractive charge–charge interactions may not play a dominant role in amyloid formation at neutral pH because β2m (isoelectric point, 6.4) and polyPs are both negatively charged. Moreover, β2m forms the native conformation, which prevents amyloid formation. Hofmeister series (Eq. **2**) showed that phosphate is one of the anions with strong hydration (33) and, thus, stabilizing effects against proteins. Thus, polyPs with a large number of phosphate groups appeared to induce amyloid fibrils based on Hofmeister effects. According to the underlying mechanism of Hofmeister effects, hydration around phosphate groups and consequent preferential hydration around exposed hydrophobic groups, which is energetically unfavorable, leads to a conformational shift to a compact conformation with less exposed hydrophobic surfaces. Among the four equilibrium conformational states expected for β2m at pH 7 (Fig. 5), the extent of the exposed surface is as follows (34):

$$\begin{aligned}\text{unfolded state} > \text{amorphous aggregate} \\ > \text{amyloid fibril} > \text{native state}.\end{aligned} \quad [4]$$

Contrary to our expectation, we did not observe the evident stabilization of the native state by polyPs monitored by urea (*SI Appendix*, Fig. S7*A*) or heat-dependent denaturation (*SI Appendix*, Fig. S7*C*); however, slight stabilizing effects were observed with $(NH_4)_2SO_4$, which was monitored by urea-induced denaturation (*SI Appendix*, Fig. S7*B*). Although significant retardation of the lag time of amyloid formation with increases in the polyP-L concentration at pH 7 and ultimate prevention at 8 mM polyP-L (Fig. 3) still argue the stabilization of the native state by polyP-L, the exact effects on the native state are unclear at this stage. On the other hand, polyP-L strongly prevented the depolymerization of amyloid fibrils prepared at pH 2 (*SI Appendix*, Fig. S7*D*). Moreover, the addition of NaCl retarded the amyloid formation (*SI Appendix*, Fig. S8). These results indicated that polyPs at neutral pH induce amyloid fibrils by the preferential stabilization of amyloid fibrils with less exposed hydrophobic surfaces over more exposed unfolded states or amorphous aggregates (Fig. 5). Possible Hofmeister effects induced by polyP may function at neutral pH irrespective of the protein net charge.

Implications for Dialysis-Related Amyloidosis. Various biological molecules have been reported to have the potential to interact with β2m to induce amyloid fibrils at neutral pH, ultimately resulting in the development of dialysis-related amyloidosis in patients (13, 21, 28). However, polyPs, which strongly induced amyloid formation at several μM at neutral pH (Fig. 3), were never previously considered as a risk factor of dialysis-related amyloidosis. On the other hand, the concentration of orthoP in the blood of patients receiving long-term hemodialysis is controlled at 3.5 to 6.0 mg/dL to prevent the formation of poorly soluble calcium phosphate. Moreover, in those patients, high serum orthoP level is strongly associated with mortality (35–37).

However, the detailed mechanism of the interactions between phosphates and tissues is incompletely understood. Furthermore, short polyPs consisting of less than a few dozen phosphate residues are often included in foods and beverages to prevent drying and improve taste. Due to the strong in vitro ability of polyPs to induce the amyloid formation of β2m at neutral pH, even at a micromolar concentration, we cannot exclude the possibility that polyPs play a role in amyloid deposition in patients receiving long-term hemodialysis. Furthermore, accumulation of phosphates is associated with acceleration of vascular calcification with the progression of kidney diseases as well as the long-term hemodialysis (38). The present results argue that it will be important to carefully examine the effects of various phosphate-related compounds including polyphosphates and calcium phosphate (39) on the development of dialysis-related amyloidosis. To achieve this goal, it will be important to establish a system that monitors the concentrations of polyPs in long-term hemodialysis patients. Concomitant increases in serum concentrations of β2m and polyPs may synergistically trigger the formation of amyloid fibrils, leading to the development of dialysis-related amyloidosis.

In conclusion, we herein found that polyPs induced the amyloid fibrils of β2m under both acidic and neutral pH conditions. PolyP-dependent amyloid formation under acidic conditions was consistent with the competitive mechanism of amyloid formation and amorphous aggregation by attractive charge–charge interactions. On the other hand, polyP-dependent amyloid formation at neutral pH was likely to occur through the strong Hofmeister effects of condensed phosphate groups. Although the pathogenic mechanism of dialysis-related amyloidosis in patients has been studied extensively, the substances responsible or mechanisms that break the supersaturation of β2m in patients remains unclear. The present results suggest an important role of polyPs in the amyloid formation of β2m in vivo, providing insights into the pathogenesis of dialysis-related amyloidosis.

Materials and Methods

Expression and purification of recombinant human β2m are described in *SI Appendix*. The formation of fibrils and amorphous aggregates was characterized by various methods including ThT fluorescence, LS, CD, and TEM. Interactions between polyPs and β2m were studied by ITC and NMR experiments. The details are described in *SI Appendix*.

ACKNOWLEDGMENTS. We thank the members of the Interdisciplinary Program for Biomedical Sciences (Osaka University) for their helpful discussions. This work was performed under the Cooperative Research Program for the Institute for Protein Research, Osaka University (CR-16-02, ICR-16-02), and was supported by the Japan Society for the Promotion of Science (15H04362, 17K07363, 17K15074, and Core-to-Core Program A), Ministry of Education, Culture, Sports, Science and Technology (16H00836, 17H06352), and Japan Agency for Medical Research and Development (16809242). J.K. was supported by the National Research, Development and Innovation Office, Hungary (K120391, 2017-1.2.1-NKP-2017-00002, TÉT_16-1-2016-0197).

1. Y. Yoshimura *et al.*, Distinguishing crystal-like amyloid fibrils and glass-like amorphous aggregates from their kinetics of formation. *Proc. Natl. Acad. Sci. U.S.A.* **109**, 14446–14451 (2012).
2. M. Adachi, M. So, K. Sakurai, J. Kardos, Y. Goto, Supersaturation-limited and unlimited phase transitions compete to produce the pathway complexity in amyloid fibrillation. *J. Biol. Chem.* **290**, 18134–18145 (2015).
3. T. Miti, M. Mulaj, J. D. Schmit, M. Muschol, Stable, metastable, and kinetically trapped amyloid aggregate phases. *Biomacromolecules* **16**, 326–335 (2015).
4. A. Nitani *et al.*, Heparin-dependent aggregation of hen egg white lysozyme reveals two distinct mechanisms of amyloid fibrillation. *J. Biol. Chem.* **292**, 21219–21230 (2017).
5. M. Adachi *et al.*, Aggregation-phase diagrams of β_2-microglobulin reveal temperature and salt effects on competitive formation of amyloids *versus* amorphous aggregates. *J. Biol. Chem.* **293**, 14775–14785 (2018).
6. D. S. Eisenberg, M. R. Sawaya, Structural studies of amyloid proteins at the molecular level. *Annu. Rev. Biochem.* **86**, 69–95 (2017).
7. R. Tycko, Physical and structural basis for polymorphism in amyloid fibrils. *Protein Sci.* **23**, 1528–1539 (2014).
8. S. Yamamoto, F. Gejyo, Historical background and clinical treatment of dialysis-related amyloidosis. *Biochim. Biophys. Acta* **1753**, 4–10 (2005).
9. J. D. Sipe *et al.*, Amyloid fibril proteins and amyloidosis: Chemical identification and clinical classification international society of amyloidosis 2016 nomenclature guidelines. *Amyloid* **23**, 209–213 (2016).
10. K. L. Moreau, J. A. King, Protein misfolding and aggregation in cataract disease and prospects for prevention. *Trends Mol. Med.* **18**, 273–282 (2012).
11. M. So, D. Hall, Y. Goto, Revisiting supersaturation as a factor determining amyloid fibrillation. *Curr. Opin. Struct. Biol.* **36**, 32–39 (2016).
12. B. Raman *et al.*, Critical balance of electrostatic and hydrophobic interactions is required for beta 2-microglobulin amyloid fibril growth and stability. *Biochemistry* **44**, 1288–1299 (2005).
13. S. L. Myers *et al.*, A systematic study of the effect of physiological factors on beta2-microglobulin amyloid formation at neutral pH. *Biochemistry* **45**, 2311–2321 (2006).
14. A. J. Doig, P. Derreumaux, Inhibition of protein aggregation and amyloid formation by small molecules. *Curr. Opin. Struct. Biol.* **30**, 50–56 (2015).
15. C. M. Cremers *et al.*, Polyphosphate: A conserved modifier of amyloidogenic processes. *Mol. Cell* **63**, 768–780 (2016).
16. K. D. Kumble, A. Kornberg, Inorganic polyphosphate in mammalian cells and tissues. *J. Biol. Chem.* **270**, 5818–5822 (1995).
17. E. Pavlov *et al.*, Inorganic polyphosphate and energy metabolism in mammalian cells. *J. Biol. Chem.* **285**, 9420–9428 (2010).
18. F. A. Ruiz, C. R. Lea, E. Oldfield, R. Docampo, Human platelet dense granules contain polyphosphate and are similar to acidocalcisomes of bacteria and unicellular eukaryotes. *J. Biol. Chem.* **279**, 44250–44257 (2004).
19. F. Müller *et al.*, Platelet polyphosphates are proinflammatory and procoagulant mediators in vivo. *Cell* **139**, 1143–1156 (2009).
20. J. H. Morrissey, S. H. Choi, S. A. Smith, Polyphosphate: An ancient molecule that links platelets, coagulation, and inflammation. *Blood* **119**, 5972–5979 (2012).
21. H. Naiki, T. Okoshi, D. Ozawa, I. Yamaguchi, K. Hasegawa, Molecular pathogenesis of human amyloidosis: Lessons from β_2-microglobulin-related amyloidosis. *Pathol. Int.* **66**, 193–201 (2016).
22. J. Hoshino *et al.*, Significance of the decreased risk of dialysis-related amyloidosis now proven by results from Japanese nationwide surveys in 1998 and 2010. *Nephrol. Dial. Transplant.* **31**, 595–602 (2016).
23. H. Naiki *et al.*, Establishment of a kinetic model of dialysis-related amyloid fibril extension in vitro. *Amyloid* **4**, 223–232 (1997).
24. M. So *et al.*, Supersaturation-limited and unlimited phase spaces compete to produce maximal amyloid fibrillation near the critical micelle concentration of sodium dodecyl sulfate. *Langmuir* **31**, 9973–9982 (2015).
25. M. So, Y. Hata, H. Naiki, Y. Goto, Heparin-induced amyloid fibrillation of β_2-microglobulin explained by solubility and a supersaturation-dependent conformational phase diagram. *Protein Sci.* **26**, 1024–1036 (2017).
26. M. Kihara *et al.*, Seeding-dependent maturation of beta2-microglobulin amyloid fibrils at neutral pH. *J. Biol. Chem.* **280**, 12012–12018 (2005).
27. S. Valleix *et al.*, Hereditary systemic amyloidosis due to Asp76Asn variant β_2-microglobulin. *N. Engl. J. Med.* **366**, 2276–2283 (2012).
28. A. Relini *et al.*, Heparin strongly enhances the formation of β_2-microglobulin amyloid fibrils in the presence of type I collagen. *J. Biol. Chem.* **283**, 4912–4920 (2008).
29. S. Yamamoto *et al.*, Low concentrations of sodium dodecyl sulfate induce the extension of beta 2-microglobulin-related amyloid fibrils at a neutral pH. *Biochemistry* **43**, 11075–11082 (2004).
30. T. Narimoto *et al.*, Conformational stability of amyloid fibrils of β_2-microglobulin probed by guanidine-hydrochloride-induced unfolding. *FEBS Lett.* **576**, 313–319 (2004).
31. Y. Goto, N. Takahashi, A. L. Fink, Mechanism of acid-induced folding of proteins. *Biochemistry* **29**, 3480–3488 (1990).
32. Y. Goto, M. Adachi, H. Muta, M. So, Salt-induced formations of partially folded intermediates and amyloid fibrils suggests a common underlying mechanism. *Biophys. Rev.* **10**, 493–502 (2018).
33. S. Nihonyanagi, S. Yamaguchi, T. Tahara, Counterion effect on interfacial water at charged interfaces and its relevance to the Hofmeister series. *J. Am. Chem. Soc.* **136**, 6155–6158 (2014).
34. T. Ikenoue *et al.*, Heat of supersaturation-limited amyloid burst directly monitored by isothermal titration calorimetry. *Proc. Natl. Acad. Sci. U.S.A.* **111**, 6654–6659 (2014).
35. B. Kestenbaum *et al.*, Serum phosphate levels and mortality risk among people with chronic kidney disease. *J. Am. Soc. Nephrol.* **16**, 520–528 (2005).
36. M. Taniguchi *et al.*; Committee of Renal Data Registry of the Japanese Society for Dialysis Therapy, Serum phosphate and calcium should be primarily and consistently controlled in prevalent hemodialysis patients. *Ther. Apher. Dial.* **17**, 221–228 (2013).
37. S. Yamada, C. M. Giachelli, Vascular calcification in CKD-MBD: Roles for phosphate, FGF23, and klotho. *Bone* **100**, 87–93 (2017).
38. S. Kobayashi *et al.*, Coronary artery calcification, ADMA, and insulin resistance in CKD patients. *Clin. J. Am. Soc. Nephrol.* **3**, 1289–1295 (2008).
39. Z. Biyik, N. Y. Selcuk, H. Z. Tonbul, M. Anil, M. Uyar, Assessment of abdominal aortic calcification at different stages of chronic kidney disease. *Int. Urol. Nephrol.* **48**, 2061–2068 (2016).